The clumped isotope geothermometer in soil and paleosol carbonate

J. Quade [a,*], J. Eiler [b], M. Daëron [c], H. Achyuthan [d]

[a] *Department of Geosciences, University of Arizona, Tucson, AZ 85721, USA*
[b] *Division of Geological and Planetary Sciences, California Institute of Technology, Pasadena, CA 91125, USA*
[c] *Laboratoire des Sciences du Climat et de l'Environnement, CNRS–CEA–UVSQ, Gif-sur-Yvette, France*
[d] *Department of Geology, Anna University, Chennai 600 025, India*

Abstract

We studied both modern soils and buried paleosols in order to understand the relationship of temperature (T°C(47)) estimated from clumped isotope compositions (Δ_{47}) of soil carbonates to actual surface and burial temperatures. Carbonates from modern soils with differing rainfall seasonality were sampled from Arizona, Nevada, Tibet, Pakistan, and India. T°C(47) obtained from these soils shows that soil carbonate forms in the warmest months of the year, in the late morning to afternoon, and probably in response to intense soil dewatering. T°C(47) obtained from modern soil carbonate ranges from 10.8 to 39.5 °C. On average, T°C(47) exceeds mean annual temperature by 10–15 °C due to summertime bias in soil carbonate formation, and to summertime ground heating by incident solar radiation. Secondary controls on T°C(47) are soil depth and shading.

Site mean annual air temperature (MAAT) across a broad range (0–30 °C) of site temperatures is highly correlated with T°C(47) from soils, following the equation:

$$\mathrm{MAAT}(^{\circ}\mathrm{C}) = 1.20(\mathrm{T^{\circ}C}(47)_0) - 21.72 \quad (r^2 = 0.92)$$

where T°C(47)$_0$ is the effective air temperature at the site estimated from T°C(47). The effective air temperature represents the air temperature required to account for the T°C(47) at each site, after consideration of variations in T°C(47) with soil depth and ground heating. The highly correlated relationship in this equation should now permit mean annual temperature in the past to be reconstructed from T°C(47) in paleosol carbonate, assuming one is studying paleosols that formed in environments generally similar in seasonality and ground cover to our calibration sites.

T°C(47)$_0$ decreases systematically with elevation gain in the Himalaya, following the equation:

$$\mathrm{elevation} \ (\mathrm{m}) = -229(\mathrm{T^{\circ}C}(47)_0) + 9300 \quad (r^2 = 0.95)$$

Assuming that temperature varied similarly with elevation in the past, this equation can be used to reconstruct paleoelevation from clumped isotope analysis of ancient soil carbonates.

We also measured T°C(47) from long sequences of deeply buried ($\leqslant 5$ km) paleosol carbonate in the Himalayan foreland in order to evaluate potential diagenetic resetting of clumped isotope composition. We found that paleosol carbonate faithfully records plausible soil T°C(47) down to 2.5–4 km burial depth, or $\sim$90–125 °C. Deeper than this and above this temperature, T°C(47) in paleosol carbonate is reset to temperatures >40 °C. We observe $\sim$40 °C as the upper limit for T°C(47) in modern

* Corresponding author. Tel.: +1 520 818 8006; fax: +1 520 621 2672.

E-mail addresses: quadej@email.arizona.edu (J. Quade), eiler@gps.caltech.edu (J. Eiler), matheiu.daeron@gmail.com (M. Daëron), hachyuthan@yahoo.com (H. Achyuthan).

soils from soil depths >25 cm, and therefore that T°C(47) >40 °C obtained from ancient soil carbonate indicates substantially warmer climate regimes compared to the present, or non-primary temperatures produced by resetting during diagenesis. If representative, this limits the use of T°C(47) to reconstruct ancient surface temperature to modestly buried (<3–4 km) paleosol carbonates. Despite diagenetic resetting of Δ_{47} values, $\delta^{18}O$ and $\delta^{13}C$ values of the same deeply buried paleosol carbonate appear unaltered. We conclude that solid-state reordering or recrystallization of clumping of carbon and oxygen isotopes can occur in the absence of open-system exchange of paleosol carbonate with significant quantities of water or other phases.

1. INTRODUCTION

Soil carbonate is abundant and widely distributed in the geologic record and has proved useful in paleoenvironmental reconstruction. For example, the $\delta^{13}C$ value of soil carbonate is widely employed in paleoecologic (e.g. Quade and Cerling, 1995) and paleo-pCO$_2$ reconstruction (Cerling, 1991). The $\delta^{18}O$ value of soil carbonate is useful for reconstructing the $\delta^{18}O$ value of meteoric water, a relationship that has seen application to paleoaltimetry (e.g. Rowley and Currie, 2006; Quade et al., 2007; Garzione et al., 2008). The clumped isotope paleothermometer is a recent development that holds potential for reconstruction of paleotemperatures in the deeper geologic record. A range of natural and synthetic calcites have been shown to yield accurate and acceptably precise (est. ±2 °C) temperatures of formation (Eiler, 2007). The question addressed in this paper is whether paleotemperatures reflecting conditions of soil carbonate formation can be similarly reconstructed using this technique.

Two considerations enter into the response to this question, the first having to do with ground heating as related to seasonality of soil carbonate formation, site shading, and site aspect; and the second with preservation of T°C(47) after burial. Soil temperature varies diurnally and seasonally in soils, and so, depending on soil depth, T°C(47) will depend on the average time of day and year that it forms. These relationships must be understood from modern soils before results from ancient soils can be interpreted. Carbonate should precipitate when dewatering of the soil and CO$_2$ out-gassing have reached the point where calcite saturation is attained in a soil water film. It stands to reason that this will happen sometime in the summer half year, when soil water content is at its lowest. Thus, soil temperatures somewhere between mean annual temperature (generally attained in the spring and fall) and warmer summer temperatures should be recorded in the calcite. The strength of this seasonal preference depends on how wet the soil becomes in spring and early summer, and how quickly soil pores dry thereafter.

This general picture of carbonate formation is supported by clumped isotope analyses of Passey et al. (2010). This study shows that soil carbonate forms in the warmer months of the year in some mid-latitude arid settings, when soil temperature exceeds mean annual temperature by at least 15 °C. Moreover, recent evidence collected by Breecker et al. (2009) suggest that carbonate in soils forms only in drought years and then only at the warmest point in the summer. If representative, it means that only extreme summer temperatures will be recorded in the soil down to

a depth of several meters. In this paper we test whether these generalizations hold for the broad range climatic settings in which soil carbonate forms.

Ground temperatures typically exceed air temperature due to heating by incident solar radiation. The flux of solar radiation in any one area varies with local slope/aspect and shading. In laterally continuous modern or ancient soils on flat topography, soil temperature should vary with shading, affording a means of reconstructing vegetation density and distribution in the past. We explore the effects of shading and aspect in our study of soils and paleosols.

The second consideration is the resistance of clumped isotopes to subsequent diagenetic resetting or reordering at elevated burial temperatures. Recent study of carbonatite carbonate (Dennis and Schrag, 2010) suggests that solid-state reordering of clumping of carbon and oxygen occurs below 250–300 °C if cooling is rapid, and <200 °C where cooling is slower. The same study showed that clumped isotopes were reordered in the apparent absence of bulk recrystallization of calcite. We test these and other conclusions by analysis of paleosol carbonates deeply (>3 km) buried over the past 12–15 million years.

1.1. Sampling modern soils

Soil carbonate forms slowly, and visible and easily sampled amounts only build up in soils over hundreds to thousands of years. For our study to succeed we had to sample soils that experienced temperatures close to today's throughout their development. Hence we confined our sampling to Holocene-age soils, since mean annual Holocene temperatures averaged over 500–1000 years (the minimum time spans averaged by our sampling) probably have not varied by more than ±1–2 °C.

There are various lines of evidence that indicate whether a given soil is Holocene in age. As a first assessment in the field, we use morphology of the soil, including degree of development of the calcic and overlying cambic horizons (Gile et al., 1966). In some areas such as Arizona and New Mexico soil development as a function of age is well established, whereas in others such as Tibet it is not, and must be inferred by morphologic comparison with well-dated sites. After samples were collected in the field, we determined the ages of their carbonates by ^{14}C dating. This and the clumped analysis requires about 10 mg of material each, which is easily acquired by scraping of clasts in soils that have experienced more than a few thousand years of pedogenesis.

It is essential that the depth of carbonate formation has remained nearly fixed through time in a given profile, be-

Table 1
Descriptions of field sites.

Site	Location	Latitude	Longtitude	Elevation (m)	Vegetation	Aspect	Stage	Soil T logging?	MAP cm/year	MAAT[*] °C	WAMT[*] °C	Summer max. daytime	T °C $(47)_0$
North America													
MAD-1,2	Madera Canyon, Arizona	N31°46.881	W110°53.176	1105	Mixed mesquite grassland	1–2°NW	I	yes	44.6	18.2	27.3/9.1	40	29.2/35.8
HUACH T2	Huachuca Mountains, Arizona	N31°27.299	W110°22.392	1910	Mixed conifer grassland	flat	I	yes	70	11.0	20.0/2.3	30	26.9
Clear Creek #1	Monitor Mountains, Nevada	N38°49.048	W116°30.134	2235	Pinyon-sagebrush desert	2–3°E-NE	I–II	yes	31.2	6.3	14.3/−1.7	31	26.7
Hawaii	Big Island near Kona				Mesquite grassland		I–III	no[a]	27.2	19.7	21/18.3	26.3	NA
Asia													
INACR 8b	Agra, Uttar Pradesh, India	N27°14.567	E77°49.883	148	NA	flat	II	no[a]	71	25.6	35/15	NA	40.1
INACR 11	Punjab, India	N29°44.315	E76°58.362	233	Grassland	flat	II	no[a]	71	24.4	33.9/15.9	NA	41.1
INACR 50	Jammu, India	N32°35.044	E74°59.406	348	NA	flat	I	no[a]	53	22.9	32.4/11.6	NA	40.6
INACR 57	Jayal, Rajasthan, India	N27°11.841	E74°18.365	340	Grass-shrub desert	flat	II	no[a]	61	25.5	33.6/15.9	NA	39.6
7893	Punjab, Pakistan	NA	NA	~500	Grassland on Potwar loess	flat	I	no[a]	94	23.5	32.8/12.4	NA	35.6
Lhasa 8	Yarlang Valley, Tibet	N29°46.675	E91°30.308	3784	Shrub-grassland	8°NW	I	yes	44.5	7.6	16.2/−2.0	20	27.8
Lhasa 9	Yarlang Valley, Tibet	N29°42.196	E91°22.437	3741	Shrub-grassland	5–6°S	I–II	yes	44.5	7.6	16.2/−2.0	20	23.8
NRT S1	Ngangla Ring Tso, Tibet	N31°20.126	E83°24.724	4800	Dwarf shrub steppe	flat	I	yes	23.5	3.0	12.1/−9	18	21.0
Lhasa-4	Yarlang Valley, Tibet	N29°38.287	E91°17.838	3809	Shrub-grassland	5°W-NW	III	no[a]	44.5	5.0	15.2/−4.7	21	21.5
TSP-19a	Tsangpo Valley, Tibet	N30°25.129	E82°46.045	4800	Sparse shrub grassland	flat	II	no[a]	25	−1.6	9.8/−11.7	16	19.1
TSP-21Ba	Tsangpo Valley, Tibet	N29°12.431	E88°18.908	4016	Shrub-grassland	11°SW	II	no[a]	NA	3.6	14.1/6.1	20	27.2
TSP-22a	Tsangpo Valley, Tibet	N29°19.076	E88°56.860	3876	Shrub-grassland	4°NW	I–III	no[a]	NA	4.6	14.8/−5.1	21	23.8

[*] MAAT: mean annual air temperature; WAMT: warmest average monthly air temperature.
[a] Site temperatures estimated from climate data.

Table 2
Carbon-14 dates from soil carbonate in surficial soils.

Sample number	AA-	JQ-	Location	$\delta^{13}C$ (PDB)	Fraction modern carbon	±	^{14}C age (years)	±	Cal years range (2s)	
Huachuca T2 94 cm	83873	780	Arizona	−7.2	0.9234	0.0034	640	30	554	667
Huach T2 80 cm	94520	2211	Arizona	−7.1	0.9427	0.0025	470	20	500	530
Clear Creek 1-45 A	94519	2210	Nevada	−5.9	0.9079	0.0025	780	20	680	730
Clear Creek 1-120c	94187	2223	Nevada	−5.2	0.6652	0.0021	3270	30	3410	3570
Lhasa 8-1 (70–80)	94523	2214	Tibet	−1.6	0.6879	0.0022	3000	30	3080	3320
Lhasa 8-1 (40–60)	94191	2228	Tibet	1.9	0.8136	0.0024	1660	20	1520	1610
INACR 57c	94188	2224	India	−3.4	0.4493	0.0020	6430	40	7280	7420
INACR 11c	94521	2212	India	0.0	0.4601	0.0020	6240	30	7030	7250
INACR-50B	94522	2213	India	1.4	0.0718	0.0017	21160	190	NA	NA
Kon09-2c	94190	2227	Hawaii	−2.0	0.5646	0.0021	4590	30	5070	5450
Kona 1c	94517	2208	Hawaii	−0.2	0.7661	0.0023	2140	20	2040	2300
Kona09-6-50B	94518	2209	Hawaii	1.7	0.8083	0.0024	1710	20	1550	1700

cause of the strong dependence of soil temperature on soil depth. Hence, the comparison of measured T°C and T°C(47) will only be valid where pedogenesis (soil carbonate formation) overprints a single depositional event or short series of events. Many soils, especially in low-sedimentation rate settings, are "cumulic", in that sediment is added in small increments, and hence the temperature experienced at any given depth evolves as the soil thickens. This process can introduce significant uncertainty in the interpretation of a carbonate clumped isotope growth temperature. Equally undesirable, soils can erode, reducing the apparent depth of carbonate formation.

How can cumulic and eroded soils be avoided? Fortunately, these situations are often apparent in the field. Where available, we selected soils underlying broad, flat surfaces to ensure against eroded profiles on the short time-scales we are concerned with here. Disconformities and heterogeneity in parent material textures are warning signs that profiles may be cumulic, and were therefore avoided. The ideal sample profile then had homogenous parent material and a regular progression of soil horizons (A–B–C) with a homogenous-looking calcic horizon confined to soil depths consistent with local mean annual rainfall.

Modern pedogenic nodules and clast coatings were collected from freshly exposed trench faces or arroyo walls. Most local bedrock or their alluvial derivatives at our soil sites are carbonate free, making it unlikely that our carbonate samples have been contaminated by detrital carbonate from local bedrock. Pedogenic carbonates were scraped from alluvial or bedrock clasts or sampled from nodules. The soil depth was recorded for all samples.

We selected study soils from a wide range of climate and soil water regimes (Table 1) to ensure that our results have broad applicability to interpreting T°C(47) from ancient soils for which seasonal soil–water status is not known. To this end, we sampled modern soils from central Nevada where rainfall in winter/spring dominated, and so soil dewatering is likely to commence in the early summer and extend into the fall. In contrast, soils in modern India, Pakistan and southern Tibet receive most of their precipitation during the summer monsoon, which for our sites commences in late June. Unlike the Nevada sites, soil–water content in our Asian study sites should be lowest just before

the monsoon begins in late June when air temperatures are at their highest. Climate in southern Arizona lies between these two extremes, characterized by a roughly equal mix of winter and summer monsoonal rainfall. Here soil water content should be lowest just before the summer rains begin in July, and again during the early fall when the summer rains stop but air temperature is still high. In equable Hawaii, seasonal air temperature variation is <3 °C, and so the range of permitted T°C(47) is narrow.

To evaluate ground-heating effects on T°C(47), we sampled soils from variably shaded ecosystems in Arizona and Nevada for comparison to virtually unshaded sites in Tibet. In Tibet we also contrasted soils sites with north versus south aspect, holding all other soil variables constant.

1.2. Sampling buried paleosols

We investigated the issue of post-burial alteration by analysis of buried paleosol carbonate from the Siwalik Group in Pakistan and Nepal. This paleosol series has been the focus of a number of previous geologic studies. The carbon and oxygen isotopic values of the paleosol carbonates are thought be primary, and to reflect on vegetation cover and climatic conditions in the past (Quade and Cerling, 1995; Quade et al., 1995). Siwalik Group paleosols are obvious targets for study because of the excellent control on age and well-constrained burial history of the thick sequences of host sediments (e.g. Johnson et al., 1985; Burbank et al., 1996). Paleosol carbonate sampled from the Siwaliks ranges in age from mid-Miocene to present, and has undergone many kilometers of burial due to high sedimentation rates in the Himalayan foreland. The carbonate occurs as discrete nodules 1–5 cm in diameter, generally in the lower half of paleosol profiles. Depth of carbonate formation during pedogenesis exceeded 50 cm for all samples analyzed.

Paleosol carbonate was sampled from the Siwalik Group section at Surai Khola in central Nepal, a section that has been studied intensively (Appel and Rösler, 1994; Quade et al., 1995; Ojha et al., 2008). The measured section thickness is about 4.5 km, and assuming average upper Siwalik sedimentation rates of ∼0.5 km/million years (Ojha et al., 2008), probably was closer to 5.5 km thick if an unmeasured thickness of conglomerate capping the section is

added. Ages of samples range from about 2.5 to 12 Ma. These deposits were rotated and exhumed <2 Ma in the hanging wall of the Main Frontal Thrust in this tectonically active area.

We obtained samples during previous studies from several different sections (Quade and Cerling, 1995) on the Potwar Plateau to assemble a burial history for our Pakistani samples. Composite thickness of the Siwalik sections in Pakistan are somewhat less certain than in Nepal but probably were on the order of 4 km, assuming sedimentation rates of 0.2 km/my for the upper portions of our sections (Burbank et al., 1996). Ages of samples range from 0.5 to about 15 Ma. These deposits are located in the in the hanging wall of the Salt Range and other major thrust faults in the region, and were probably rotated and exhumed <1 Ma.

2. METHODS

2.1. Soil monitoring

Modern soils sampled for carbonate were first dug out to about one meter depth, and soil temperature and humidity loggers (Hobo(@) Pro v2) installed at 20–30 cm depth, and at 90–100 cm depth. An additional logger was placed in a nearby tree or shaded location to record air temperature. These recorded temperature and relative humidity every 2 h for 1–2 years, to be later recovered and the data downloaded.

Soil and air temperature data was recovered from about half of the sites we sampled for clumped isotope analysis in this study (Table 1). For the other sites, we estimated air temperatures by compiling temperature data from nearby weather stations. Where both sources of data are available, temperature estimates from weather station data are within 1–3 °C of measured mean annual and seasonal air temperatures from loggers (when appropriately averaged over time; Table 1).

2.2. Laboratory methods

Carbonates analyzed for $\delta^{18}O$ and $\delta^{13}C$ values were heated at 250 °C for 3 h *in vacuo* before stable isotopic analysis using an automated sample preparation device (Kiel III) attached directly to a Finnigan MAT 252 mass spectrometer at the University of Arizona. Measured $\delta^{18}O$ and $\delta^{13}C$ values were corrected using internal laboratory standards that were previously calibrated to NBS-19. The external reproducibility of repeated analyses of standards averaged $\pm 0.11‰$ for $\delta^{18}O$ (1σ). Carbonate $\delta^{18}O$ and $\delta^{13}C$ values are reported using standard δ-per mil notation relative to VPDB.

About 15 mg of carbonate was set aside for ^{14}C analysis on select samples from each profile. These were converted to CO_2 and then graphite using standard procedures, and then measured at the University of Arizona Accelerator Mass Spectrometry facility (Donahue et al., 1990).

Clasts set aside for clumped-isotope analysis were rinsed with de-ionized water and dried using compressed air. Carbonate coatings were scraped off the clasts using a stainless

steel dental pick, then ground and homogenized in an agate mortar. This carbonate was not heated prior to analysis, unlike carbonate used for $\delta^{18}O$ and $\delta^{13}C$ determinations. Clumped-isotope compositions of these carbonate powders were analyzed at the California Institute of Technology using protocols described by Ghosh et al. (2006a), Affek and Eiler (2006) and Huntington et al. (2009). Seven to ten mg aliquots were digested overnight at 25 °C in anhydrous orthophosphoric acid. After cryogenic trapping, the resulting CO_2 was purified of potential isobaric contaminants by passage through a dry ice/ethanol slush and a 30-m-long 530 μm ID Supelco GC column held at –10 °C. CO_2 was then analyzed using a Finnigan MAT 253 dual-inlet mass spectrometer configured for isotope ratio measurements of masses 44–49. Bulk composition ($\delta^{13}C$ and $\delta^{18}O$) was computed from these measurements using a reference CO_2 tank of known isotopic composition. Clumped isotope results are reported using standard Δ_{47}-per mil notation, derived from comparison with heated gases, i.e. CO_2 in a thermodynamic state of nearly randomly distributed isotopes (with $\Delta_{47} \sim$ est. 0.025), obtained by heating CO_2 aliquots at 1000 °C. Data are reported in tables both in the Caltech intra-laboratory reference frame (similar to most previous papers on carbonate clumped isotope thermometry) and the recently proposed 'Imperial', or absolute, reference frame of Dennis et al. (2011). Data referenced to the Caltech intra-laboratory frame was used to throughout the text and figures.

3. RESULTS AND DISCUSSION

3.1. Modern soils

3.1.1. Carbon-14 results

With one exception, ^{14}C dates from soil carbonate returned Holocene ages, ranging in age, after conversion to calendar years, from $\sim$7350 to 500 years BP (Table 2). The single exception was a soil from India in which the age is 21,160 ^{14}C years BP. This generally confirms our assumption that the sampled carbonates formed in temperature and rainfall conditions similar to today.

3.1.2. Soil temperature – general considerations

Before presenting our results from modern soils, it is useful to review the relationship between soil and air temperature. This topic is addressed in any basic soil physics text, and can be briefly summarized as follows. Soil temperature (T) varies with time (t) and exponentially as function soil depth (z) following (from Hillel, 1982):

$$T(z,t) = T_{avg} + A_o[\sin(\omega t - z/d)]/e^{z/d} \tag{1}$$

where T_{avg} is average air temperature, A_o is the amplitude of seasonal or diurnal temperature variation (maximum minus minimum) at the soil surface (z = 0), ω is radial frequency (respectively, 2π year^{-1} and 2π day^{-1}), z is soil depth, d is the "damping" depth (or 1/e folding depth) characteristic of the soil:

$$d = (2\kappa/C_v\omega)^{1/2} \tag{2}$$

where κ is thermal conductivity and C_v is volumetric heat capacity. As regards surface-T fluctuations, the $1/e$ folding depth, d, of diurnal fluctuations on the order of centimeters – much shallower than the average depth of carbonate accumulation. This means that at shallow depths (<30 cm) in soils, temperatures varies significantly on a daily basis, but at depth ($\sim$30–300 cm), diurnal fluctuations are damped out, and seasonal swings in soil temperature dominate down to a depth (depending on local soil properties) of about 300 cm (Fig. 1). Below $\sim$300 cm, soil temperature is nearly invariant seasonally, and the seasonal swings in soil temperature collapse to a value close to mean annual temperature.

This simple description of soil temperature lacks one additional key effect, that of ground heating of soils by incident solar radiation. The equations above assume that soils will heat to no higher than the overlying air column. This situation generally obtains in full shade but not in soils exposed to sunlight. Soils cannot advect in response to heating, and will thus heat up compared to overlying air when exposed to sunlight. These ground-heating effects are visible in all the temperature logger data, from the completely bare soils of Tibet (Fig. 2a–c) to the variably shaded soils of Arizona (Fig. 2d–e). Many studies also document this effect, such as Breshears et al. (1998) or Bartlett et al. (2006), who found that the difference between ground and air temperature increased with observed solar radiation by 1.2 K/100 W m^{-2}.

A number of our samples underlie slopes of >5°, allowing us to assess the effects of slope and aspect on soil heating. For example, sites Lhasa 8 and 9 lie between 3700 and 3800 m across the Yarlung valley from each other. Despite similar elevations, soil temperature data shows that Lhasa 9, south facing on a 5–6° slope, is $\sim$2–3 °C warmer during summer at 100 cm depth than soil at Lhasa-8, northwest facing along a 8° slope.

3.1.3. T°C(47) results

Two patterns in T°C(47) are visible in most soil profiles we sampled (Table 3), excluding results from Hawaii, which we will consider separately below. First, our results show that T°C(47) exceeds that of local mean annual air temperature (MAAT) by large amounts ranging from about +4 to +22 °C, for an average difference of $\sim$+12 °C (Fig. 3a). T°C(47) is much closer to warmest average monthly temperatures (WAMT), generally exceeding WAMT by +2–3 °C (Fig. 3b). Scatter in T°C(47) at a given MAAT (or WAMT) can be attributed to depth variation in T°C(47), as discussed below.

Second, most, but not all, profiles show decreasing T°C(47) with soil depth. The profiles from site NRT in Tibet (Fig. 2c) and Huachuca T2 (Fig. 2d) in Arizona are examples of this. T°C(47) at NRT increases from 13.7 °C to 24.7 °C from 95 ± 5 to 35 ± 5 cm soil depth; whereas at Huachuca T2, average T°C(47) increase from 20.1 °C at 130 cm to 23.4 °C at 70 cm soil depth.

In other locations, depth patterns are mixed. For example, at the MAD sites in Arizona, two profiles were sampled from different locations in the same alluvial terrace (Fig. 2e). At MAD-2, the depth pattern in T°C(47) is scattered and in all cases lower than at MAD-1. At MAD-1, T°C(47) shows a noticeable decrease with increasing soil depth, and T°C(47) near the surface is high, well above summer maximum air temperature.

We suggest that the overall patterns in observed T°C(47) indicate that clumped isotope temperatures of soil carbonates generally reflect equilibrium growth, but at temperatures that differ, sometimes markedly, from mean annual temperatures due to seasonality of growth and ground heating. This view is inspired by the common pattern of decreasing T°C(47) with soil depth – the predicted pattern for summer seasons in all studied soils – and by measured summer soil temperatures approaching or overlapping measured T°C(47). The details of measurements from profiles
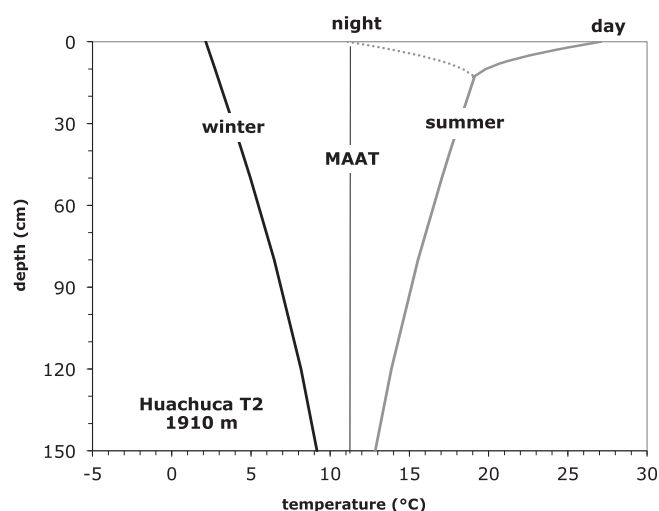

Fig. 1. Typical modeled seasonal and diurnal soil temperature patterns, in this case for site Ft. Huachuca T2, formed under the site conditions given in Table 1.
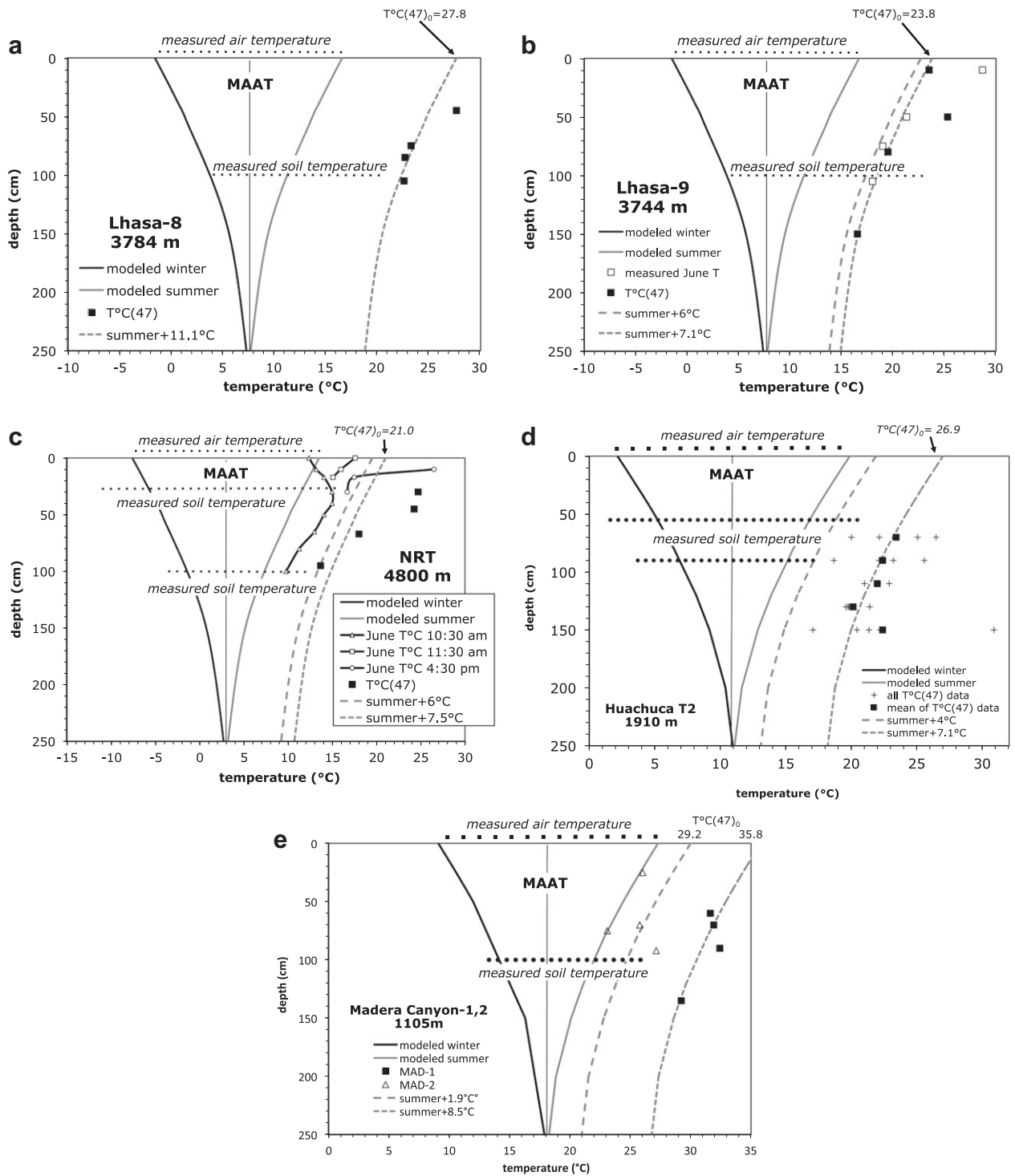
Fig. 2. Individual modern soil site results plotted against soil depth, showing mean annual temperature (MAAT), modeled winter and summer soil temperatures (solid black and gray curves) and summer soil temperature with added ground heating (dashed curves), measured (by temperature loggers) soil and air temperature (dotted horizontal lines, based on monthly means for air temperature and 2-hourly measurements for soil temperature), and measured T°(47) (solid squares). Estimates of T°C(47)$_0$ also shown at upper right, where best-fit summer soil temperature curves intersect the soil surface. For sites in Tibet: (a) Lhasa-8, (b) Lhasa-9, with June afternoon soil temperatures measured with a thermometer, (c) NRT, with June daytime soil temperatures measured with a thermometer; and in Arizona: (d) Ft. Huachuca T2, and (e) Madera Canyon, in which soil temperature logger data (horizontal dotted line) comes from a semi-shaded site near MAD-2.

Table 3
Isotope and isotopologue results from surficial soils.

Sample	Sample depth (cm)	Carbonate %	$\delta^{13}C$ (PDB)	$\delta^{18}O$ (PDB)	Δ_{47} Caltech reference frame	T°C(47)	Δ_{47} Absolute reference frame[*]
Arizona-Madera Canyon							
M1P-60-Aa	60		−8.0	−8.3	0.62	31.6	0.67
M1-70-Aa	70		−8.1	−8.2	0.62	31.9	0.67
M1P-90-Aa	90		−7.5	−8.4	0.61	32.4	0.66
M1-135-Aa	135		−8.5	−7.7	0.63	29.2	0.68
M2-25-Ab	25		−8.7	−6.0	0.64	26.0	0.69
M2-70-Aa	70		−8.7	−6.5	0.64	25.8	0.69
M2-75-Aa	75		−8.7	−6.3	0.65	23.1	0.71
M2-92-Aa	92		−8.4	−6.9	0.64	27.2	0.69
Arizona-Fort Huachuca							
H-70-Aa	70		−6.4	−7.9	0.64	26.4	0.69
H-70-Ba	70		−8.4	−9.7	0.65	25.0	0.70
H-70-Bb	70		−8.5	−10.1	0.67	20.0	0.72
H-70-Ca	70		−8.3	−10.0	0.66	22.1	0.71
H-90-Aa	90		−6.9	−8.9	0.65	23.2	0.71
H-90-Ba	90		−7.2	−8.8	0.66	22.1	0.71
H-90-Bb	90		−7.2	−8.8	0.64	25.5	0.69
H-90-Bc	90		−7.2	−8.8	0.68	18.6	0.73
H-110-Aa	110		−7.8	−10.1	0.66	22.9	0.71
H-110-Ba	110		−7.9	−8.6	0.66	21.0	0.72
H-110-Bb	110		−7.9	−8.5	0.66	22.0	0.71
H-130-Aa	130		−8.2	−8.9	0.67	19.8	0.72
H-130-Ba	130		−8.5	−8.8	0.67	19.7	0.72
H-130-Bb	130		−8.5	−8.8	0.67	19.6	0.72
H-130-Ca	130		−7.7	−8.7	0.66	21.4	0.71
H-150-Ba	150		−8.7	−7.1	0.62	30.8	0.67
H-150-Bb	150		−8.6	−7.9	0.66	21.3	0.71
H-150-Bc	150		−8.6	−7.9	0.68	17.1	0.74
H-150-Ca	150		−8.4	−8.3	0.67	20.4	0.72
H-150-Cb	150		−8.4	−8.4	0.66	22.2	0.71
Nevada-Clear Creek							
CLCR1-75a	75		−4.3	−16.2	0.59	39.5	0.63
CLCR1-120A	120	85	−3.9	−14.0	0.66	22.5	0.71
CLCR1-120D	120	84	−5.2	−11.1	0.67	18.8	0.73
CLCR1-45A	45	63	−6.4	−11.4	0.65	24.3	0.70
Hawaii-Kona							
KONA 09-1C		16	0.1		0.63	27.6	0.68
KONA 09-1C		27	0.0	−4.8	0.56	46.1	0.61
KONA 09-4B(2)		23	−2.6	−3.6	0.68	17.8	0.73
KONA 09-2B		35	−4.5	−6.5	0.59	38.5	0.64
India							
INACR 57(b)	250	55	−3.0	−5.7	0.62	30.4	0.67
INACR 50(a)	85	31	−3.1	−6.4	0.60	36.4	0.65
INACR07 11A(a)	175	51	−0.5	−6.3	0.62	31.3	0.67
INACR 50(b)	85	60	2.0	−3.8	0.60	35.0	0.65
INACR 8bBK1	150	29	−2.8	−6.5	0.61	32.5	0.66
INARC 57(a)			−3.0	−5.7	0.62	30.2	0.67
INACR 11(b)	175		−0.5	−6.0	0.60	34.8	0.65
Pakistan							
7893–30-40 cm	35 ± 5		1.4	−5.8	0.62	31.3	0.67
7893–50 cm	50		1.7	−6.1	0.63	29.4	0.68
7893–125 cm	125		1.4	−5.8	0.62	31.4	0.67
Tibet							
Lhasa 8-1	45 ± 5		−2.6	−17.0	0.63	27.8	0.68
Lhasa 8-2	75 ± 5		−1.9	−17.8	0.65	23.4	0.70
Lhasa 8-3	85 ± 5		−1.2	−17.2	0.66	22.8	0.71
Lhasa 8-4	105 ± 5		−1.6	−18.9	0.66	22.7	0.71

Table 3
(*Continued*)

Sample	Sample depth (cm)	Carbonate %	$\delta^{13}C$ (PDB)	$\delta^{18}O$ (PDB)	Δ_{47} Caltech reference frame	T°C(47)	Δ_{47} Absolute reference frame[*]
Lhasa 9-1	10 ± 5		NA	NA	0.65	23.5	0.70
Lhasa 9-2	50 ± 5		NA	NA	0.64	25.3	0.70
Lhasa 9-3	80 ± 5		NA	NA	0.67	19.5	0.72
Lhasa 9-4	150 ± 5		NA	NA	0.69	16.5	0.74
NRT 25/35	30 ± 5		NA	NA	0.65	24.7	0.70
NRT 40/50	45 ± 5		NA	NA	0.65	24.3	0.70
NRT 65/70	65 ± 5		NA	NA	0.68	18.0	0.73
NRT 90/100	95 ± 5		NA	NA	0.70	13.7	0.75
L-4a	58 ± 12		−1.8	−17.9	0.68	17.2	0.73
L-4b	58 ± 12		−2.1	−18.0	0.68	18.6	0.73
TSP-19a	110 ± 12		3.2	−14.1	0.71	11.6	0.76
TSP-19b	110 ± 12		7.3	−11.7	0.71	10.8	0.77
TSP-21Ba	50 ± 5		−4.4	−18.8	0.65	23.5	0.70
TSP-21Bb	50 ± 5		−4.5	−19.2	0.66	21.6	0.71
TSP-21Bc	50 ± 5		−4.2	−19.0	0.64	26.0	0.69
TSP-22a	60 ± 10		0.3	−18.4	0.66	21.8	0.71
TSP-22b	60 ± 10		0.3	−18.3	0.68	17.7	0.73

[*] Calculated using a secondary standardization, using assumed Δ_{47} values for carbonate standards and 1000 °C heated gases. These values are provided only as a guide to interlaboratory comparison and were not used to calculate reported temperatures.

like NRT and Lhasa-9 especially influence our interpretation. Values of T°C(47) from >50 cm soil depth in both profiles (Fig. 2c for NRT and Fig. 2b for Lhasa-9) closely approach measured June soil temperatures, just before the cooling effects of the monsoon rains arrive. Patterns like these point to a common and pronounced seasonal bias of T°C(47): carbonate in the studied sections is only forming in the warmest part of the warmest month, before the rains and when soil dewatering, largely by plants, is probably most intense.

Values of T°C(47) between 0 and 50 cm display a more varied pattern that we interpret to reflect diurnal temperature fluctuations. Temperature measurements at site NRT (Fig. 2c) with a digital thermometer show diurnal variations on a summer afternoon in the upper 50 cm of the soil. The distribution of T°C(47) matches this pattern and points to formation in this soil in the afternoon, mostly similar to an average formation time of ∼4 pm. The systematic depth offset in temperatures suggests that the carbonate formed on warmer average afternoons than that of our single afternoon of measurements. The profile of T°C(47) values for site Lhasa-9 (Fig. 2b) is more complicated but could be interpreted as reflecting carbonate formation between the late morning (10 cm) to late afternoon (50 cm). This view assumes that carbonate throughout the profile forms over the same seasonal interval of time, when soils are driest.

We also suggest that the uniformity of the patterns of T°C(47) profiles in the studied Tibet soils is the result of the bareness of the soils now and in the past. Aside from very scant low shrub and herb cover, the Tibet soils are quite bare. Vegetation reconstructions argue against significant woody cover at our sites during the Holocene (Kaiser et al., 2009; Pelletier et al., 2011). In short, the Tibet sites have always been unshaded, and the thermal response of the soils to solar radiation should have been spatially and temporally similar from year to year.

In contrast, our monitoring sites from Arizona and Nevada are more vegetated and therefore locally cooled by shade. At the Clear Creek site (2235 masl), the vegetation is dominated by large sagebrush (*Artemesia tridentata*) interspersed with pinyon (*Pinus monophylla*) and juniper (*Juniperus osteosperma*) trees. At the Arizona sites, mixed mesquite (*Prosopis velutina*), white-thorn acacia (*Acacia constricta*), and summer C_4 grasses dominate the MAD sites (1105 masl), whereas alligator-bark juniper (*Juniperus deppeana*), white oak (*Quercus arizonica*), and tall C_4 grasses cover the Huachuca T2 site (1910 masl). Local vegetation cover on these alluvial terrace sites probably varied over the thousand year time scales of soil carbonate formation – more shaded for some periods of time at any one spot, and less for other periods. It is not clear how we can evaluate the integrated effects of shade from place to place, but the effects of shade on soil temperature are well documented. Intercanopy areas in nearby New Mexico experience near-surface soil temperatures 10 °C higher than shaded areas (Breshears et al., 1998). Changes in local shading could therefore explain the discrepancy in measured soil temperatures today and T°C(47), as well as the large difference in T°C(47) from profiles MAD-1 and MAD-2 (Fig. 2e). These profiles came from the same alluvial terrace only a few hundred meters apart, and yet T°C(47) in MAD-2 (more shaded throughout its formation?) is lower than in MAD-1 (less shaded?). It is difficult to see how this hypothesis of variable shading through time could be clearly proven or disproven. We simply suggest this as a plausible consequence of variations in ground temperature in variably vegetated sites, insofar as T°C(47) from the MAD-1 matches the high ground temperatures in bare locations in this area, whereas those of MAD-2 resemble air (i.e. = completely shaded) temperatures.

Sites Lhasa 8 and 9 were sampled to test for the potential effects of aspect on ground heating. The sites are similar

in elevation, parent material, and lack of vegetation, and only differ in that Lhasa-8 is on the toe of an alluvial fan dipping ∼8° northwest, and Lhasa-9 5–6° south. This probably explains why summertime ground temperatures at Lhasa-9 exceed that of Lhasa-8 by ∼2–3 °C, as measured over parts of two summers. However, we found that T°C(47) for Lhasa 8 exceeds that of Lhasa 9 by about 3 °C, which given their aspect, is the opposite of expectation. Whatever the cause, it is noteworthy that two unshaded sites experiencing about the same air temperature differ by in T°C(47) by ∼3 °C. The role of aspect and slope on soil heating bears further investigation; but soils should probably be avoided where significant depositional paleoslopes (such as rocky alluvial fans) are likely.

In the analysis above we have excluded our limited results from Hawaiian soils, but nonetheless present the analyses in Table 3. The Hawaiian soil carbonate from three profiles displays very large variation in T°C(47) of 28 °C, much greater than any other area, even though Hawaiian climate is the most equable of our sites. Moreover, one T°C(47) result of 46 °C is the highest value by 7 °C that we obtained from any modern soil. We see two possible explanations for these unusual results. Unlike other sites, the Hawaiian soils are developed entirely on Quaternary basalt flows on the semi-arid (Kona) side of the island of Hawaii. The carbonate is dolomitic, and heavily admixed with non-carbonates (>80% silicates and other salts). In most cases the "soil" carbonate was obtained from fracture faces in open fissures in the young basalt flows. Our concern with these samples is that carbonate likely forms in fissures partially open to advecting air, more like a cave than a soil in which soil carbonate forms slowly and with restricted gas exchange with air. Kinetic, nonequilibrium effects on clumped isotopes are well documented for caves (Affek et al., 2008; Daëron et al., 2011).

Alternatively, the results from the Hawaiian soils could be recording true soil temperatures. The lowest T°C(47) result at 18 °C is within error of mean annual air temperature at the site of 19.7 °C (Table 1). The much higher T°C(47) of 39–46 °C may reflect extreme surface heating of the exposed black basalt surfaces, more efficiently translated to depth by the 2x higher density of basalt compared to most soils. Until the soil temperature loggers are recovered from Hawaii in 2013, and the possibility of kinetic effects is thoroughly addressed, we have excluded the Hawaiian results from our synthesis.

3.1.4. Reconstructing air temperature from T°C(47)

The objective in this section is to establish relationships between T°C(47) and more familiar temperatures terms such as mean annual air temperature (MAAT) and warmest average monthly air temperature (WAMT). It is important to recall that daily and seasonal air temperatures attenuate significantly with soil depth, a pattern visible in our T°C(47) results as well. Thus, the correlation of raw T°C(47) results, uncorrected for soil depth, to any more general climatic parameters such as MAAT is modest ($r^2 = 0.62$) at shallow (<100 cm) soils depths, but improves ($r^2 = 0.93$) deeper (>100 cm) in soil where soil temperature variations smooth out (Fig. 3). These relationships should prove useful to those studies where original soil depth is only broadly constrained (e.g. Ghosh et al., 2006b).

A more powerful approach is to "correct" all T°C(47) results for soil depth from a single soil profile. In this case we can draw a best-fit model curve through a single or, better, a series of T°C(47) values with soil depth (Fig. 2). These best-fit curves are calculated using equations 1 and 2 as follows:

(1) assume a thermal conductivity ($\kappa = 0.0007$ cal cm^{-1} s^{-1} °C^{-1} and a volumetric heat capacity (C_v) = 0.3 cal cm^{-1} °C^{-1}. These values are typical of dry, sandy soils. In the absence of ground heating this produces the "modeled summer" temperature-depth profile in Figs. 1 and 2.
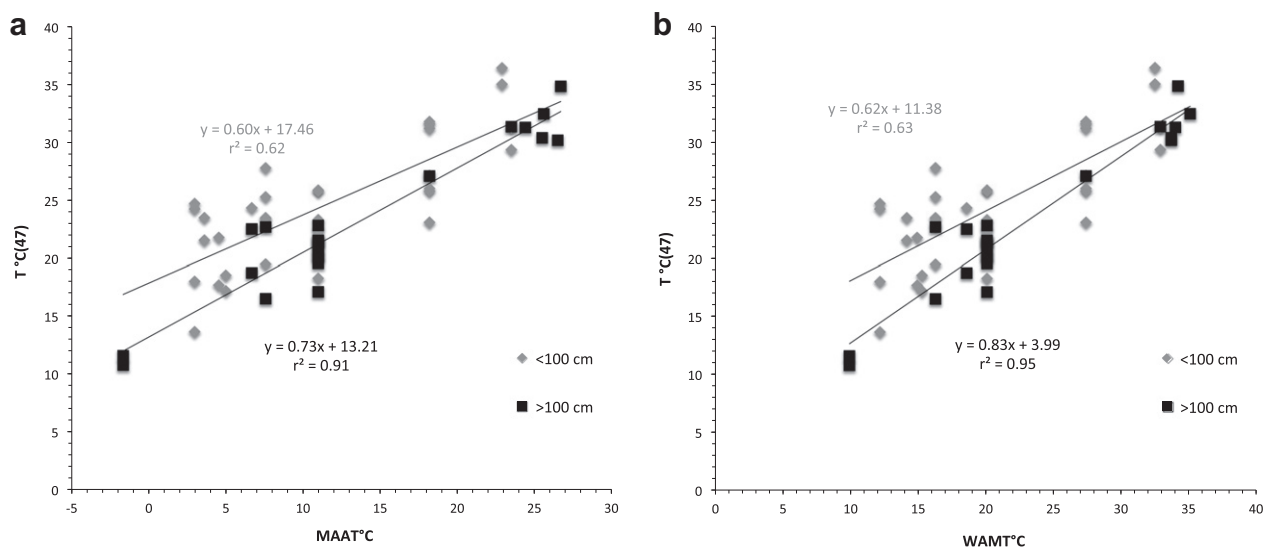

Fig. 3. Plot of T°C(47) versus (a) mean annual temperature (MAAT) and (b) warmest average monthly air temperature (WAMT) from <100 cm and >100 cm soil depths, for all global sites except Hawaii.

(2) to account for ground heating, add to T_{avg} in Eq. (1) until the curve from step (1) above fits the observed array of T°C(47) values with soil depth. The best fit is obtained by the sum of least squares using only sample points $\geqslant 50$ cm deep, to avoid any diurnal heating effects. We refer to the intersection of such a fitted model curve with the soil surface as the "effective surface temperature", or $T°C(47)_0$, required to fit the underlying soil temperature profile (Fig. 2). In this way, a single $T°C(47)_0$ can be calculated from a single or series of T°C(47) values with soil depth. Note that $T°C(47)_0$ should be expected to exceed WAMT by the degree of ground heating, anywhere from 0 to 6 °C depending on shading.

(3) We compared local air temperature to our estimates of $T°C(47)_0$ from our global sampling of modern soils. From this we observe strong correlations of $T°C(47)_0$ with MAAT (Fig. 4a) and WAMT (Fig. 4b) as follows:

$$\text{MAAT °C} = 1.20^{*}T°C(47)_0 - 21.72 \quad (r^2 = 0.92) \quad (3)$$
$$\text{WAMT °C} = 1.13^{*}T°C(47)_0 - 10.81 \quad (r^2 = 0.89) \quad (4)$$

These are important results that have implications for reconstructing paleotemperatures in the past. At face value, they mean that T°C(47) collected from a paleosol depth profile can be used to reconstruct $T°C(47)_0$, which in turn can be used to reconstruct mean annual temperature as well as seasonality of temperature in the past. The most robust estimates of $T°C(47)_0$ will come from analysis of multiple samples >50 cm deep, although single samples >50 cm also provide very usable constraints on $T°C(47)_0$. Depth-resolved sampling profiles also should provide useful information on seasonality.

But it is important at this point not to overstate the universality and usefulness of these results; more work is needed. First, our sampling of modern soils, although quite broad, involves climates with very strong seasonality and variable shading. In more equable climates where MAAT and WAMT are close together, these relationships are going to be different, as shown by Passey et al. (2010) in East Africa. In East Africa, average monthly temperatures vary by <4 °C, far less than with our study sites, which are almost all >20 °C except for Hawaii (Table 1). As a result, T°C(47) is closer to MAAT in East Africa than in our sites. For equable climates, we would predict that the difference between $T°C(47)_0$ and WAMT will be the same as for our more seasonal soils, but a much smaller difference between $T°C(47)_0$ and MAAT. The lesson here is that some independent knowledge of paleoseasonality is desirable before T°C(47) can be interpreted. Analysis of complete paleosol profiles of T°C(47) over several meters would serve this end, since the degree of depth attenuation in T°C(47) should scale with seasonality.

Shade is a key imponderable for interpreting T°C(47). The strong difference in T°C(47) between MAD-1 and MAD-2 could be taken as an illustration of the effects of shade. The slope of best-fit lines between the air temperature and $T°C(47)_0$ (Fig. 4) is 1.1–1.2, rather than 1:1. This may be influenced by the greater bareness of cold climate soils compared to warm climate soils in our study. Analysis of well-shaded cold climate soils and thinly vegetated soils in warms settings would be a useful test. With more calibration (and as clumped isotope analysis becomes easier or at least more common), paleoshade may one day prove reconstructable, and its effects corrected for in Eqs. (3) and (4). Looking farther ahead, it is conceivable that vegetation patchiness (i.e. paleoshade) could be reconstructed by comparing T°C(47) profiles laterally from the same paleosols.

Moreover, all of our modern study sites experience dry conditions for at least part of the summer, although most (Arizona, Tibet, India. Pakistan) also receive significant rainfall later in the summer. Thus, T°C(47) is biased toward the summer months, as already discussed. If, however, a
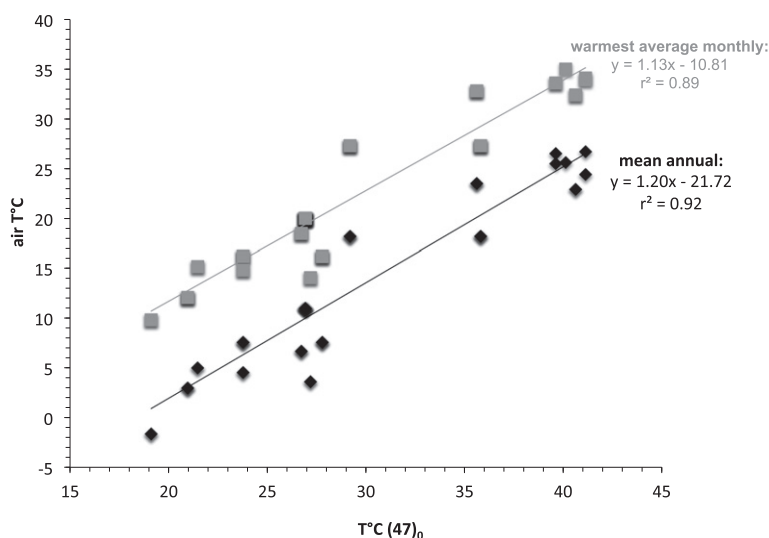

Fig. 4. Plot of mean annual air temperature (MAAT) and warmest average monthly air temperature (WAMT) versus $T°C(47)_0$ required by a modeled best fit of measured T°C(47) with soil depth, for all global sites except Hawaii.

soil does not dry out in summer due to precipitation all through the summer half year, then T°C(47) might form at temperatures at or below mean annual temperature. Persistent summer wetness may explain the cool soil temperatures recorded by Δ_{47} values in low-elevation (<2 km) soil carbonate from central Andes in Argentina (Peters et al., 2012). These observations challenge the universality of our conclusions concerning hot summer conditions for soil carbonate formation. We speculate that this exception should develop only in mid-latitude settings such as central Argentina where winters are cool and dry, and summers persistently wet; but not at high (summer dry) and low latitudes (winter warm).

3.1.5. T°C(47) lapse rates for Himalaya–Tibet

There is intense interest in the paleoaltimetry of the Himalaya and Tibet (e.g. Rowley and Currie, 2006; Quade et al., 2011). T°C(47) is sure to play a role in these reconstructions, and here we provide an interpretive framework for those future efforts. We have merged the Indian, Pakistani, and Tibetan results in Fig. 5. There is a strong correlation between elevation versus T°C(47)$_0$:

$$\text{elevation (m)} = -229(\text{T°C(47)}_0) + 9300 \quad (r^2 = 0.95) \quad (5)$$

This amounts to a soil temperature lapse rate of -4.4 °C/km, less than average free air lapse rates of -5 to -6 °C/km, probably because the low-elevation Indian soils are cooled by vegetation cover, but high-elevation Tibetan soils are not.

3.2. Buried paleosols and diagenesis

Thin sections of paleosol carbonate nodules from Siwalik sections reveal dominantly micrite with minor cross-cutting veins of sparry calcite, for samples from a broad range of burial depths. The fine textures are typical of primary nodular soil carbonate and are generally accepted as evidence against major recrystallization during burial (Garzione et al., 2004; Leier et al., 2009).

T°C(47) from buried Siwalik paleosol carbonate at Surai Khola in Nepal range from 24 to 60 °C (Table 4; Fig. 6). There is a clear pattern of increasing T°C(47) with depth. Paleosols in the upper ~2.5 km (or <5.5 Ma) of the section yield temperatures of <34 °C, consistent with T°C(47) from modern Indian soil carbonate from across the border in India (Table 3). At burial depths > 4 km (or > 6.5 Ma), T°C(47) exceeds 36 °C, with most values >40 °C.

There is a very similar pattern of increasing T°C(47) with age and depth from paleosol carbonates sampled from Pakistan (Table 4 and Fig. 7). Paleosol carbonates <6 Ma yield T°C(47) of <37 °C, similar to modern soil carbonate from the area (29–31 °C) whereas T°C(47) is almost all 35–53 °C in paleosol carbonate >9 Ma. The burial depths are less certain in Pakistan than Nepal, but we estimate that the reset samples at ~9 Ma underwent ~2 km of burial, and the deepest and oldest samples were buried ~4 km.

Maximum likely burial temperatures can be estimated using observed geothermal gradients of 20–30 °C/km from Siwalik basins in Pakistan (Khan and Raza, 1986). Assuming an average geothermal gradient of ~25 °C/km, our results show that resetting of Δ_{47} values may commence at maximum burial temperatures as low as around 80–90 °C, but certainly by 125 °C. The resetting is incomplete, since the highest T°C(47) is 60 °C, and peak burial temperatures were likely >125 °C. Samples yielding T°C(47) > 40 °C are in the 7–17 Ma range. They were gradually buried over the past 12–15 million years, then exhumed rapidly in the last 1–2 million years in the hanging wall of frontal thrusts (the Salt Range Thrust in Pakistan and Main Frontal Thrust in Nepal) in the distal Himalayan foreland. It is not clear by what mechanism the clumped isotope composition of these soil carbonates are partially reset. However, prior experimental study of resetting of the carbonate clumped isotope thermometer by heating in the absence
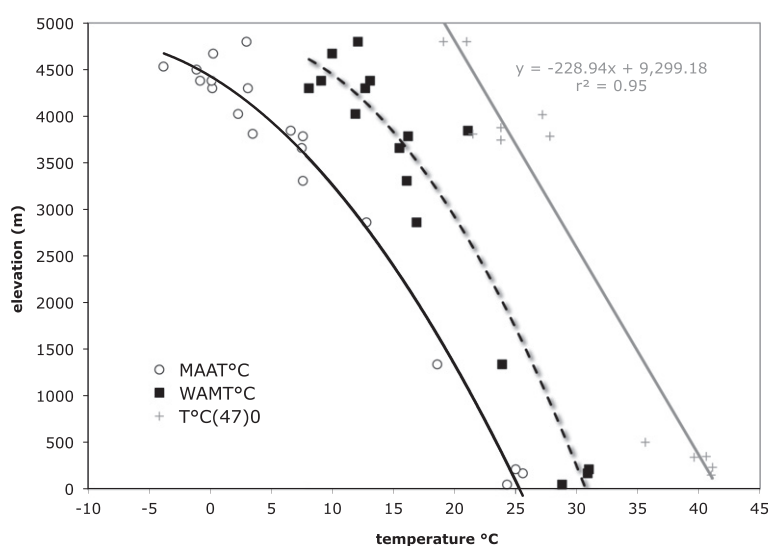

Fig. 5. Plot of changes with elevation (in meters) along the Himalayan front in relation to mean annual temperature (MAAT), to warmest average monthly air temperature (WAMT), and to estimated T°C(47)$_0$ from modern soils in India and Tibet. Equation of best fit line for elevation (y) versus T°C(47)$_0$ (x) shown.

Table 4
Isotope and isotopologue results from buried paleosols.

Sample	Age (Ma)	Burial depth (m)	Carbonate %	$\delta^{13}C$ (PDB)	$\delta^{18}O$ (PDB)	Δ_{47} Caltech reference frame	T°C (47)	Δ_{47} Absolute reference frame[*]
Nepal								
SK-71	1.1	964	57	2.6	−5.3	0.65	23.9	0.70
SK70	1.3	1034		−10.3	−7.1	0.65	24.7	0.70
SK-67	1.7	1079		1.1	−6.6	0.62	30.4	0.67
SK-63	3.2	1697	42	0.7	−6.4	0.63	27.7	0.68
SK-60	3.6	1866		0.5	−6.3	0.65	24.9	0.70
SK-58	3.9	1953		−5.0	−8.1	0.63	27.5	0.69
SK-50	4.2	2081		1.5	−7.0	0.61	32.6	0.66
SKC-16	4.3	2102		2.0	−6.7	0.63	27.5	0.69
SK-46	4.7	2274		0.5	−6.8	0.66	22.7	0.71
SK-43	4.7	1461		−7.2	−7.0	0.65	25.0	0.70
SK-42	5.0	2374		2.5	−8.5	0.63	28.7	0.68
SK-40	5.1	2415		2.1	−7.0	0.59	38.5	0.64
SK-37	5.2	2463		1.0	−7.7	0.61	34.0	0.66
SK-30	5.9	2749		−0.9	−8.0	0.61	33.5	0.66
SK-26	6.8	3284		−10.1	−7.5	0.60	35.8	0.65
SK-9	7.8	3923	33	−10.6	−8.6	0.59	37.7	0.64
SK-16	7.8	3706		−12.1	−8.9	0.57	43.8	0.62
SK-73	9.8	4328	37	−9.3	−7.8	0.52	56.6	0.57
SK-75	10.0	4407		−10.1	−9.1	0.57	44.6	0.61
SK75	10.0	4407		−10.1	−9.1	0.56	47.5	0.60
SK-81	10.5	4605		−10.5	−7.6	0.57	42.8	0.62
SK-83	11.5	4960		−9.7	−6.5	0.58	40.8	0.63
SK-22 20 min rxn 90C	6.5	3477		−7.4	−11.2	0.55	49.1	0.60
SK-22 1 h rxn 90C	6.5	3477		−7.5	−11.1	0.52	58.1	0.57
SK-22, 5 min rxn 90C	6.5	3477		−7.5	−11.3	0.53	54.9	0.58
SK-22, 19 h rxn at 25C	6.5	3477		−7.6	−9.5	0.51	59.7	0.56
SK-22, 2 h 3% H2O2	6.5	3477		−7.7	NA	0.53	56.1	0.57
Pakistan								
9220	0.6	NA	35	0.6	−6.8	0.64	25.2	0.70
9210	1.1	NA		2.4	−6.7	0.60	34.9	0.65
9191	1.7	NA		3.0	−4.6	0.61	33.2	0.66
7905b	1.8	NA	46	−0.6	−4.8	0.63	28.0	0.68
8051	2.5	NA		1.2	−5.1	0.62	31.2	0.67
8024	3.1	NA	53	0.4	−6.9	0.65	24.3	0.70
9646	5.9	NA	46	−0.1	−7.3	0.63	29.5	0.68
9143	9.3	NA	55	−9.1	−9.3	0.55	48.2	0.60
9154	9.3	NA		−7.0	−8.6	0.61	33.5	0.66
9126	9.6	NA	54	−9.5	−8.7	0.60	36.1	0.65
7934	9.8	NA		−11.3	−8.6	0.60	36.6	0.65
7933	9.9	NA		−9.5	−9.6	0.59	37.6	0.64
7929	10.1	NA		−9.9	−8.9	0.60	36.3	0.65
7919	10.4	NA		−10.3	−9.7	0.58	40.1	0.63
7916	11.4	NA		−9.3	−9.7	0.57	42.7	0.62
9819	11.6	NA		−9.7	−9.6	0.57	43.0	0.62
7862	13.3	NA		−9.2	−10.1	0.54	51.3	0.59
9135	14.4	NA	57	−10.3	−9.3	0.58	40.4	0.63
7893–30-40 cm	0	surface		1.4	−5.8	0.62	31.3	0.67
7893–50 cm	0	surface		1.7	−6.1	0.63	29.4	0.68
7893–125 cm	0	surface		1.4	−5.8	0.62	31.4	0.67

[*] Calculated using a secondary standardization, using assumed Δ_{47} values for carbonate standards and 1000 °C heated gases. These values are provided only as a guide to interlaboratory comparison and were not used to calculate reported temperatures.
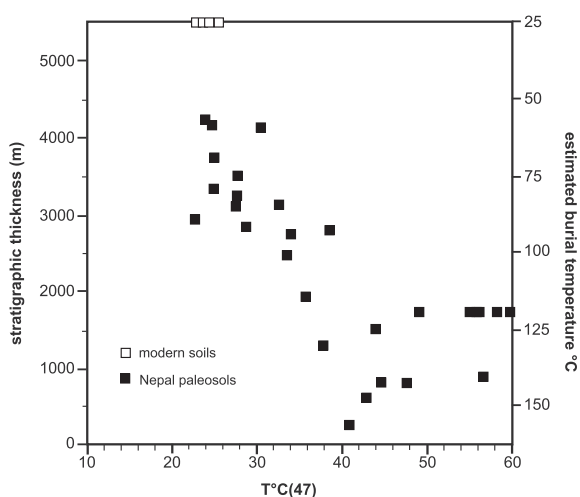
Fig. 6. Plot of T°C(47) versus estimated burial temperature and stratigraphic thickness of paleosol carbonate samples from the Siwalik Group at Surai Khola in south-central Nepal (see Table 4 for more information on samples). Burial temperature was estimated using a geothermal gradient of 25 °C/km and a mean annual surface temperature of 25 °C. T°C(47) for the modern soil carbonate (Table 1, INACR- samples) from nearby sites in north India is plotted for comparison.
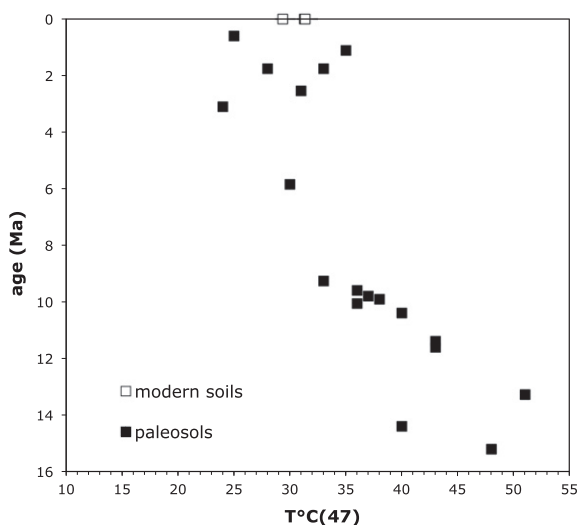

Fig. 7. Plot of T°C(47) versus age of paleosol carbonate samples from the Siwalik Group in Punjab, Pakistan (see Table 4 for more information on samples). T°C(47) for the modern soil carbonate (Table 1, sample 7893) is plotted for comparison. The oldest paleosols were probably buried as much as 4 km.

of recrystallization, and prior analyses of slowly cooled marbles, suggest that the blocking temperature with respect to diffusive re-equilibration is on the order of 150–200 °C. And the apparent activation energy for this diffusive re-equilibration mechanism is sufficiently high that very little change should occur at even modestly lower temperatures. Therefore, it appears that partial resetting of soil carbonates on burial in the range ~2.5–5 km reflects recrystalliza-

tion rather than solid-state diffusion. This inference should be tested through detailed studies of the fabrics and trace element geochemistry of partially reset, deeply buried soil carbonates.

A natural question is whether the well-documented increase after 8 Ma in $\delta^{18}O$ and $\delta^{13}C$ values from paleosol carbonate in these sections is related to the diagenetic resetting experienced by clumped isotopes across about the same burial depth range. We would argue that resetting of clumped isotopes is not accompanied by resetting of $\delta^{18}O$ and $\delta^{13}C$ records from the same paleosols. The $\delta^{18}O$ and $\delta^{13}C$ records thus remain robust archives of paleoclimate and paleovegetation in the past (Quade and Cerling, 1995; Quade et al., 1995), including the first documentation of the late Miocene expansion of C_4 plants that we now know was a global event at low latitudes. The large decrease in $\delta^{13}C$ values in these sections starting ~8 Ma has been reproduced from organic matter in the same sections and in other regional records such as the Bengal Fan (France-Lanord and Derry, 1994). Likewise, the ~3‰ decrease in $\delta^{18}O$ values in paleosol carbonate samples 6–8 Ma is also documented in the $\delta^{18}O$ value of pedogenic clays in the Pakistan Siwaliks (Stern et al., 1997). This and other evidence presented in Quade and Cerling (1995) and Quade and Roe (1999) argue against diagenetic resetting of the $\delta^{18}O$ and $\delta^{13}C$ records from deeply buried paleosol carbonates. Given our suggestion that resetting of clumped isotopes was likely accomplished by recrystallization, this implies that diagenetic resetting occurred in rock-buffered, relatively fluid-poor conditions. Mora et al. (1998) and Leier et al. (2009) show that resetting of $\delta^{18}O$ values in paleosol carbonate begins where burial exceeds 4 km (>100–120 °C) and certainly by 10 km (~250 °C).

4. A FEW RECOMMENDATIONS AND BROADER IMPLICATIONS

There are a number of broader implications of our results. Key among them is that if soil carbonate does indeed form in clumped isotope equilibrium with soil temperature as the evidence indicates, it happens at peak summer temperatures. Breecker et al. (2009) and Passey et al. (2010) have already suggested that the isotopic composition of soil carbonate is summer biased. Many previous studies have assumed carbonate formation (e.g. Cerling and Quade, 1993; Mack and Cole, 2005; Dworkin et al., 2005) at or near mean annual temperature. Among other things, this temperature underestimation means that the $\delta^{18}O$ values of soil water have been overestimated, and hence the extent of soil water evaporation also overestimated. For example, the 10–15 °C difference between MAAT and T°C(47) observed in this study leads to a 3–4‰ overestimate of soil water $\delta^{18}O$ values. Moreover, as pointed out by Breecker et al. (2009), the summer bias in soil carbonate formation also means that the $\delta^{13}C$ values will over-represent the proportion of C_4–C_3 biomass compared to year-round conditions. It also means that soil carbonate tends to form under low soil pCO_2 conditions when soils are dewatered and plants stressed, potentially leading to overestimates of atmospheric pCO_2 in the past using the soil carbonate

pCO_2 paleo-barometer (Cerling, 1991; Breecker et al., 2010).

Our results show that T°C(47) in Miocene paleosol carbonate undergoes partial resetting after burial to depths of 2–4 km, where the sediment may attain temperatures of 80–115 °C. This is toward the low end of the temperature or burial range of reordering estimated by Dennis and Schrag (2010) for carbonatites and Eiler et al. (2006) for soil carbonates. In agreement with Dennis and Schrag (2010), $\delta^{18}O$ values do not undergo alteration in these conditions, in spite of recrystallization or solid-state reordering of Δ_{47} values. Huntington et al. (2011) also presented evidence for resetting of Δ_{47} in the 95–120 °C range of most but not all carbonate in Eocene-age limestone from the Colorado Plateau. The elevated temperatures developed because of nearby emplacement of basalt rather than burial.

Finally, we are optimistic about the potential for reconstructing paleotemperatures of the past from T°C(47) in soil carbonate, provided samples are not too deeply buried. Fine-grained soils should be used over coarse alluvial soils to avoid the effects of slope and aspect on soil temperature. Pedogenically "simple" profiles should be sampled to increase the likelihood that carbonate formed at observed paleosol depths. It is imperative that paleosol depth be recorded in order to calculate T°C(47)$_0$. Single samples can provide useful constraints on local paleo-air temperature, but the best estimates of T°C(47)$_0$ will come from multiple depth-resolved analyses from a single paleosol profile. T°C(47) values collected over paleosol depth profiles to reconstruct T°C(47)$_0$ will have to be corrected for compaction effects if burial has been substantial. Finally, multiple profiles from single paleosols should be sampled to evaluate effects of paleoshade. Clearly, such intensive analysis will benefit from automation and other possible innovations in carbonate clumped isotope measurements, making Δ_{47} measurements faster and more routine.

ACKNOWLEDGMENTS

REFERENCES

Affek H. P. and Eiler J. M. (2006) Abundance of mass-47 CO_2 in urban air, car exhaust and human breath. *Geochim. Cosmochim. Acta* **70**, 1–12.

Affek H. P., Bar-Mathews M., Ayalon A., Mathews A. and Eiler J. M. (2008) Glacial/interglacial temperature variations in Soreq cave speleothems as recorded by 'clumped isotope' thermometry. *Geochim. Cosmochim. Acta* **72**, 5351–5360.

Appel E. and Rösler W. (1994) Magnetic polarity stratigraphy of the Neogene Surai Khola section (Siwaliks, SW Nepal). *Himalayan Geol.* **15**, 63–68.

Bartlett M. G., Chapman D. S. and Harris R. N. (2006) A decade of ground-air temperature tracking at Emigrant Pass Observatorym Utah. *J. Clim.* **19**, 3722–3731.

Breshears D. D., Nyhan J. W., Heil C. E. and Wilcox B. P. (1998) Effects of woody plants on microclimate in a semi-arid woodland: soil temperature and evaporation in canopy and intercanopy patches. *Int. J. Plant Sci.* **159**(6), 1010–1017.

Breecker D. O., Sharp Z. and McFadden L. (2009) Seasonal bias in the formation and stable isotopic composition of pedogenic carbonate in modern soils from central New Mexico. *Geol. Soc. Am. Bull.* **121**(3/4), 630–640.

Breecker D. O., Sharp Z. D. and McFadden L. D. (2010) Atmospheric CO_2 concentrations during ancient greenhouse climates were similar to those predicted for A.D. 2100. *Proc. Natl. Acad. Sci. USA* **107**, 576–580.

Burbank D., Beck R., and Mulder T. (1996) The Himalayan foreland basin. In *The Tectonics of Asia* (eds. A. Yin and T. M. Harrison). Cambridge Univ. Press, New York. pp. 149–188.

Cerling T. E. (1991) Carbon dioxide in the atmosphere: evidence from Mesozoic and Cenozoic paleosols. *Am. J. Sci.* **291**, 371–400.

Cerling T. E. and Quade J. (1993) Stable carbon and oxygen isotopes in soil carbonates. In *Continental Indicators of Climate* (eds. P. Swart, J. A. McKenzie, and K. C. Lohman). Proceedings of Chapman Conference, Jackson Hole, Wyoming, American Geophysical Union Monograph **78**, 217–231.

Daëron M., Guo W., Eiler J., Genty D., Blamart D., Boch R., Drysdale R., Maire K., Wainer G. and Zanchetta G. (2011) $^{13}C^{18}O$ clumping in speleothems: observations from natural caves and precipitation experiments. *Geochim. Cosmochim. Acta* **75**(12), 3303–3317.

Dennis K. J. and Schrag D. P. (2010) Clumped isotope thermometry of carbonitites as an indicator of diagenetic alteration. *Geochim. Cosmochim. Acta* **74**, 4110–4122.

Dennis K. J., Affek H. P., Passey B. H., Schrag D. P. and Eiler J. M. (2011) Defining the absolute reference frame for clumped isotope studies of CO_2. *Geochim. Cosmochim. Acta* **75**, 7117–7131.

Donahue D. J., Jull A. J. T. and Toolin L. J. (1990) Radiocarbon measurements at the University of Arizona AMS facility. *Nucl. Instrum. Methods Phys. Res., Sect. B* **52**(3–4), 224–228.

Dworkin S. I., Nordt L. and Atchley S. (2005) Determining terrestrial paleotemperatures using the oxygen isotopic composition of pedogenic carbonate. *Earth Planet. Sci. Lett.* **237**, 56–68.

Eiler J. M., Garzione C. and Ghosh P. (2006) Response to comment on Rapid Uplift of the Altiplano revealed through $^{13}C–^{18}O$ bonds in paleosol carbonates. *Science* **314**, 760c. http://dx.doi.org/10.1126/science.1133131.

Eiler J. M. (2007) "Clumped-isotope" geochemistry – the study of naturally occurring multiply-substituted isotopologues. *Earth Planet. Sci. Lett.* **262**, 309–327.

France-Lanord C. and Derry L. A. (1994) $\delta^{13}C$ of organic carbon in the Bengal Fan: source evolution and transport of C_3 and C_4 plant carbon to marine sediments. *Geochim. Cosmochim. Acta* **58**(21), 4809–4814.

Garzione C. N., Dettman D. L. and Horton B. K. (2004) Carbonate oxygen isotope paleoaltimetry: evaluating the effect of diagenesis on paleoelevation estaimtes for the Tibetan Plateau. *Palaeogr. Palaeocl. Palaeoecol.* **212**, 119–140.

Garzione C. N. and seven others (2008) The Rise of the Andes. *Science* **320**, 1304–1307.

Ghosh P., Adkins J., Affek H., Balta B., Guo W., Schauble E. A., Schrag D. and Eiler J. M. (2006a) $^{13}C–^{18}O$ bonds in carbonate minerals: a new kind of paleothermometer. *Geochim. Cosmochim. Acta* **70**, 1439–1456.

Ghosh P., Eiler J. M. and Garzione C. (2006b) Rapid uplift of the Altiplano revealed in abundances of $^{13}C–^{18}O$ bonds in paleosol carbonate. *Science* **311**, 511–515.

Gile L. H., Peterson F. F. and Grossman R. B. (1966) Morphological and genetic sequences of carbonate accumulation in desert soils. *Soil Sci.* **101**(5), 347–360.

Hillel D. (1982) *Introduction to Soil Physics*. Academic Press, New York.

Huntington K. W., and ten others (2009) Methods and limitations of 'clumped' CO_2 isotope (Δ_{47}) analysis by gas-source isotope ratio mass spectrometry. *J. Mass Spectrometry* **44**, 1318–1329.

Huntington K. W., Budd D. A., Wernicke B. P. and Eiler J. M. (2011) Clumped isotope thermometry to constrain the crystallization temperature of diagenetic calcite. *J. Sediment. Res.* **81**, 656–669.

Johnson N. M., Stix J., Tauxe L., Cerveny P. F. and Tahirkhlei R. K. (1985) Paleomagnetic chronology, fluvial processes, and tectonic implications of the Siwalik deposits near Chinji village, Pakistan. *J. Geol.* **93**, 27–40.

Leier A., Quade J., DeCelles P. and Kapp P. (2009) Stable isotopic results from paleosol carbonate in south Asia: paleoenvironmental reconstructions and selective alteration. *Earth Planet. Sci. Lett.* **279**, 242–254.

Kaiser K., Opgenoorth L., Schoch W. H. and Miehe G. (2009) Charcoal and fossil wood from palaeosols, sediments and artificial structures indicating Late Holocene woodland decline in southern Tibet (China). *Quat. Sci. Rev.* **28**, 1534–1556.

Khan M. A. and Raza H. A. (1986) The role of geothermal gradients in hydrocarbon exploration in Pakistan. *J. Petrol. Res.* **9**(3), 245–258.

Mack G. H. and Cole D. R. (2005) Geochemical model of $\delta^{18}O$ of pedogenic calcite versus latitude and its application to Cretaceous palaeoclimate. *Sediment. Geol.* **174**, 115–122.

Mora C. I., Sheldon B. T., Elliot W. C. and Driese S. G. (1998) An oxygen isotope study of illite and calcite in three Appalachian Paleozoic vertic paleosols. *J. Sediment. Res.* **68**(3), 456–464.

Ojha T. P., DeCelles P. G., Butler R. F. and Quade J. (2008) Magnetic polarity stratigraphy of the Neogene Siwalik Group and Dumri Formation. *Nepal. Basin Res.*. http://dx.doi.org/10.1111/j.1365-2117.2008.00374.x.

Passey B. H., Levin N. E., Cerling T. E., Brown F. H. and Eiler J. M. (2010) High-temperature environments of human evolution in East Africa based on bond-ordering in paleosol carbonates. *Proc. Natl. Acad. Sci. USA* **107**(25), 11245–11249.

Pelletier J. D., Quade J., Goble R. J. and Aldenderfer M. S. (2011) Widespread hillslope gullying on the southeastern Tibetan Plateau: Human or climate-change induced? *Geol. Soc. Am. Bull.* **123**(9–10), 1926–1938.

Peters N. A., Huntington K. W. and Hoke G. (2012) Hot or not? Impact of seasonally variable soil carbonate formation on paleotemperature and O-isotope records from clumped isotope thermometry. *Earth Planet. Sci. Lett.* 10.1016/j.epsl.2012.10.024.

Quade J. and Cerling T. E. (1995) Expansion of C4 grasses in the late Miocene of northern Pakistan: evidence from stable isotopes in paleosols. *Palaeogr. Palaeocl. Palaeoecol.* **115**, 91–116.

Quade J. and Roe L. (1999) The stable isotopic composition of early diagenetic cements from sandstone in paleoecological reconstruction. *J. Sediment. Res.* **69**, 667–674.

Quade J., Cater J. M. L., Ojha T. P., Adam J. and Harrison T. M. (1995) Dramatic carbon and oxygen isotopic shift in paleosols from Nepal and late Miocene environmental change across the northern Indian sub-continent. *Geol. Soc. Am. Bull.* **107**, 1381–1397.

Quade J., Garzione C. and Eiler J. (2007) Paleosol carbonate in paleoelevation reconstruction. In *Paleoelevation: Geochemical and Thermodynamic Approaches* (ed. M. Kohn). Rev. Mineral. Geochem. Mineral. Soc. Am. Bull. **66**, 53–87.

Quade J., Breecker D., Daëron M. and Eiler J. M. (2011) The Paleoaltimetry of Tibet: an isotopic perspective. *Am. J. Sci.* **311**, 77–115.

Rowley D. B. and Currie B. S. (2006) Palaeo-altimetry of the late Eocene to Miocene Lunpola basin, central Tibet. *Nature* **439**, 677–681.

Stern L. A., Chamberlain C. P., Reynolds R. C. and Johnson G. D. (1997) Oxygen isotope evidence of climate change from pedogenic clay minerals in Himalayan molasse. *Geochim. Cosmochim. Acta* **61**(4), 731–744.

Associate editor: Edwin Schauble